

# Numerical simulation of wave impact with air cavity effects

Bingyue Song<sup>1</sup>, Chongwei Zhang<sup>2</sup>

1. Department of Electric Power Engineering, Kunming University of Science and Technology, Kunming 650504, China
2. State Key Laboratory of Coastal and Offshore Engineering, Dalian University of Technology, Dalian 116023, China  
Email: bingyue\_song@163.com; chongweizhang@dlut.edu.cn

## 1 Introduction

The wave impact on a structure usually starts from a single contact point, followed by a rapid change of the free surface profile and velocity. In boundary element simulations, extremely small spatial elements and temporal steps are required to capture the flow details in the local impact zone, which poses a major technical challenge. Several techniques have been proposed to deal with the difficulty. For example, Tanizawa and Yue<sup>[1]</sup> truncated the wave front into a flat-headed profile. Zhang et al.<sup>[2]</sup> and Greco et al.<sup>[3]</sup> used the self-similar impact model, by approximating the wave front as a liquid wedge with constant velocity.

In this work, we shall propose a multi-scale algorithm to simulate the complete process of wave deformation from overturning to impacting. The key technique is a simultaneous computation of the local impact zone in a stretched coordinate system and the overall wave plunging in the physical coordinate system. The air, after trapped in a cavity between an overturning wave and the structure, can be compressed adiabatically, so that the air pressure only depends on its volume. A case study is carried out for the problem of wave impact on a coastal wall with air entrapment. The characteristics and effects of the air cavity are discussed under different conditions.

## 2 Methodology

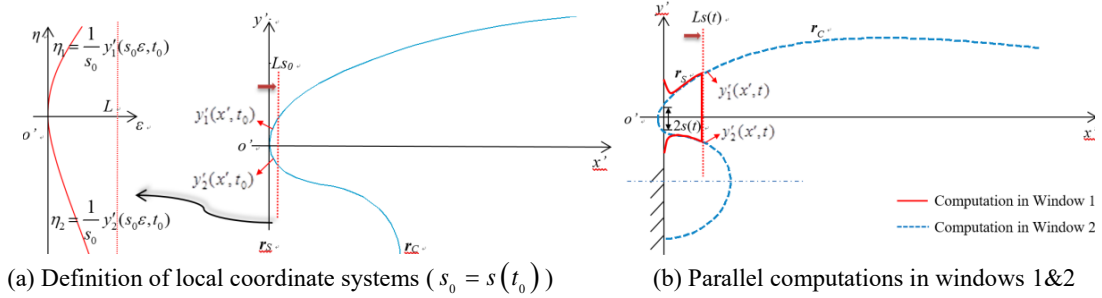


Fig. 1. Sketch of the multi-scale algorithm.

Potential-flow theory that assumes the fluid to be inviscid, incompressible and flow-irrotational is used, and the velocity potential  $\phi$  is introduced to describe the water flow. Fig. 1 shows the sketch of the multi-scale algorithm. Upon impact, a local coordinate system  $o' - x'y'$  is established with its origin located at the contact point. The  $x'$  axis is perpendicular to the impact surface pointing towards the water, and the  $y'$  axis is along the impact surface. It is 'stretched' to a new coordinate system  $o' - \epsilon\eta$  (see Wu et al.<sup>[4]</sup>) according to

$$\epsilon = x'/s, \quad \eta = y'/s \quad (1)$$

where  $s$  is the stretching ratio defined as  $s(t) = \frac{1}{2} [y'_1(x', t) - y'_2(x', t)]|_{x'=0}$ . Here,  $y'_1(x', t) > 0$  and  $y'_2(x', t) < 0$  denote the two branches of wave crest above and below the  $x'$  axis, which keeps propagating as if the impact did not happen. The velocity potential in the two local coordinate systems follows

$$\phi(x', y', t) = Us\phi(\epsilon, \eta, t) \quad (2)$$

where  $U$  is chosen the magnitude of the horizontal velocity of the contact point upon impact.

Initially, we let the wave pass through the wall for a very tiny duration  $t_0$  (which can be set as small as we want, e.g.  $t_0 = 10^{-5}$  in the simulation below), to obtain two intersection points. Set the computation domain in  $o' - \epsilon\eta$  as  $\epsilon \in [0, L]$ . This means the domain between  $x' \in [0, Ls_0]$  ( $s_0 = s(t_0)$ ) in  $o' - x'y'$  is initially transferred to the stretched coordinate system (see Fig. 1(a)). Then  $\nabla^2\phi = 0$  is solved in  $o' - \epsilon\eta$  for the local impact region (in Window-1), and  $\nabla^2\phi = 0$  is solved in  $o' - x'y'$  for the global wave transformation immune to the impact (in Window-2). At any instant after  $t = t_0$ , solutions around  $x' = Ls(t)$  from Window-2 are used

as the updated boundary conditions at around  $\varepsilon = L$  in Window-1. This is based on the assumption that the local impact does not significantly affect the flow away from the impact zone.  $L = 3$  is used in the simulation. Once the wetted surface on the wall grows sufficiently visible, Window-1 can be merged into Window-2 for a global domain simulation.

### 3 Results and discussions

We now consider the case of an overturning wave impact on a vertical seawall. The shoaling wave model described in Cooker and Peregrine<sup>[5]</sup> is applied on the initial wave boundaries to generate the impact situation in concern. Defining a 2D Cartesian system  $o-xy$  with the  $x$  axis pointing right along the still water surface and the  $y$  axis vertically pointing upwards along the wall, the horizontal velocity of the flow averaged along the vertical direction takes the form (the still water depth  $h$ , gravity acceleration  $g$  and water density  $\rho$  are used as the basis for nondimensionalisation)

$$\bar{u}(x) = -\frac{1}{2}u_0\{1 + \tanh[k(x-x_0)]\} \quad (3)$$

The initial free surface shape and velocity potential are obtained based on Airy's wave theory (e.g. Mei<sup>[6]</sup>).

#### 3.1 Initial impact stage

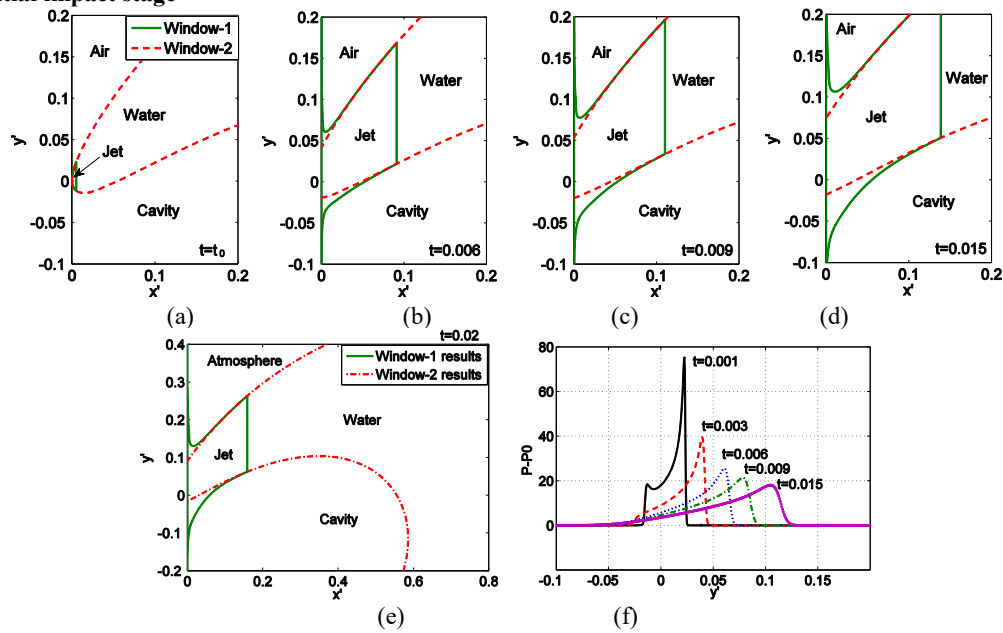


Fig. 2. Results of initial impact from  $t_0 = 10^{-5}$  to  $t = 0.02$ : (a)-(e) free surface profiles obtained from windows 1&2; (f) impact pressure on the wall (relative to the atmospheric value).

With  $u_0 = 1.1623$ ,  $k = 0.5$  and  $x_0 = 10$  in Eq. (3), the numerical simulation yields a situation of overturning wave impact on the wall with a velocity of  $(-2.625, -0.771)$  at the contact point, entrapping an air cavity of initial size  $V_0 = 0.3438$ . Results of the local impact are given in Fig. 2. From the free surface profiles shown in Figs. 2(a)-(e), it can be seen that, results obtained from the two windows are well overlapped after a small distance away from the impact zone. This confirms the earlier hypothesis that the local impact has no major effect on the far-field flow. The pressure distribution in Fig. 2(f) shows two extreme points at  $t = 0.001$ , corresponding to the positions of the upper and lower jet roots. Physically, near the intersection of the wall and the original incident wave surface, the path of the fluid particle is blocked by the wall, and it has to take a sharp turn to move away along the wall. The blocked region, similar to a stagnation point, corresponds to a local pressure extreme. The sharp turn of the fluid particle means a large acceleration which corresponds to a large pressure gradient. Away from this point, the fluid will move with large speed in a thin jet and the pressure there is close to the ambient value. As the impact continues, the overall pressure drops and the lower pressure peak diminishes quickly.

#### 3.2 Air entrainment effect

At  $t = 0.02$ , the stretching ratio increases to  $s = 0.053$ , and the overall simulation can be carried out in the physical system. The effect of the entrapped air is investigated with different values of initial non-dimensional

air pressure  $P_0$  ( $P_0 = P_a / \rho gh$ , where  $P_a = 1.01325 \times 10^5 \text{ Pa}$  is the atmospheric pressure,  $\rho = 1025 \text{ kg/m}^3$  is the water density, and  $g = 9.8 \text{ m/s}^2$  is the gravitational acceleration). When  $P_0 = 100.87$ , 10.087 and 2.017 are considered, they correspond to initial water depths of 0.1m, 1m and 5m respectively at the wall. The adiabatic law indicates  $P = P_0 (V_0/V)^\gamma$  in the cavity, where  $V$  is its volume with  $V_0$  as the initial value, and  $\gamma = 1.4$  is the heat ratio of air.

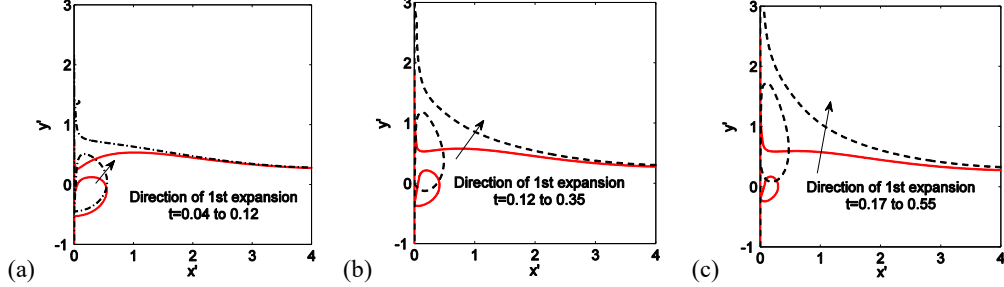


Fig. 3. The first expansion stage of the air cavity with  $P_0$  of (a) 100.87, (b) 10.087 and (c) 2.017.

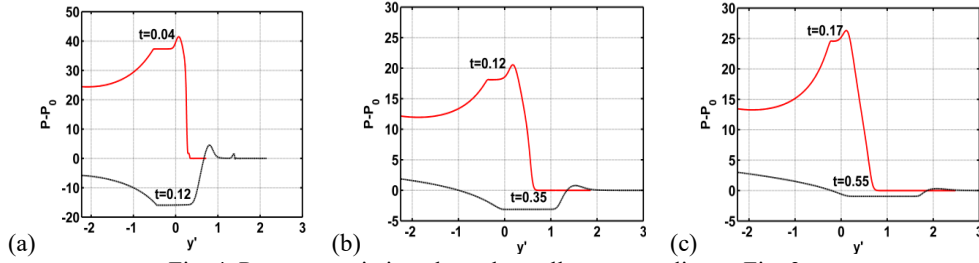


Fig. 4. Pressure variation along the wall corresponding to Fig. 3.

For the three cases, Fig. 3 depicts the process during which the air cavity rebounds from its minimum volume, after compressed by the incoming wave, to its maximum volume. Fig. 4 shows the corresponding pressure distribution along the wall. It can be seen that, the smaller  $P_0$  is, the harder and over a longer period the air cavity is compressed. A stronger rebound motion of the air cavity is then followed, and the upper wave surface rises up more violently. This agrees with the phenomenon of the much more violent upward water jet observed in larger scale experiments (e.g. Bullock et al.<sup>[7]</sup>). The smaller minimum volume of the air cavity indicates a larger value of  $P_{\max}/P_0$  (1.38, 2.80 and 13.19 respectively for the three cases), where  $P_{\max}$  denotes the maximum cavity pressure. In fact, from the conservation law of energy, we have

$$\left(\frac{P_{\max}}{P_0}\right)^{\frac{\gamma-1}{\gamma}} + (\gamma-1)\left(\frac{P_{\max}}{P_0}\right)^{\frac{1}{\gamma}} - \gamma = -\frac{\delta K + \delta E_G}{P_0 V_0 / (\gamma-1)} \quad (4)$$

where  $\delta K$  and  $\delta E_G$  refer to the change in the kinetic and gravitational potential energy of the water flow from impact to the time when the cavity is compressed to its minimum volume. Compared to the large variation in  $P_0$  in the three cases, the change in the total mechanical energy (non-dimensional) of the water,  $-(\delta K + \delta E_G)$ , may be neglected, since  $\delta K < 0$  and  $\delta E_G > 0$  in the current situation and they both increase in magnitude with smaller  $P_0$ .

At the end of the first expansion stage, the minimum cavity pressures drop to -16, -3 and -1 below the atmospheric value respectively. Meanwhile the pressure peak on the wetted surface located near the root of the upper cavity jet stays positive (refer to Fig. 4). Consequently, there is a large pressure gradient across the local fluid layer. As long as the cavity starts to re-contract, the local fluid particles are accelerated toward the inner cavity surface, generating an inner jet with free surface on both sides. This happens in each case, as shown in Fig. 5. The tendency to generate secondary inner jets, caused by the described local pressure gradient at the end of the following expansion stages, is also observed in the first two cases, as shown in Fig. 6. They are much weaker compared to the first one, due to the damping in the cavity oscillation and the decrease in the pressure peak on the original wetted surface above. While for the case  $P_0 = 2.017$ , the simulation stops at  $t = 0.76$ , when the inner jet touches the nearby cavity surface (see Fig. 5(c)). Multi-cavities could be formed after such

inner jets impinge the nearby surface, which demands further investigation.

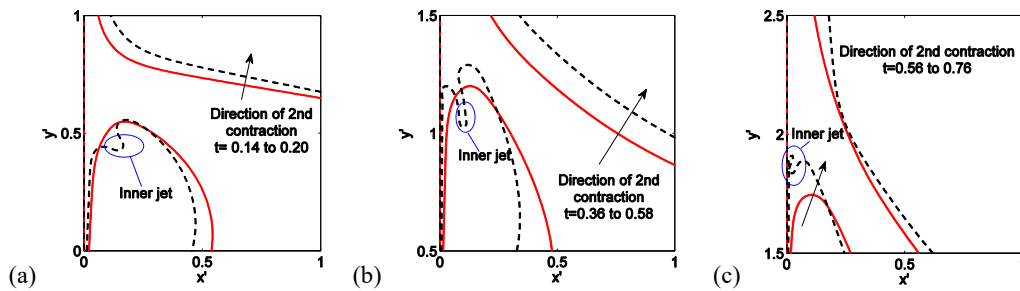


Fig. 5. Generation of inner jet during the 2<sup>nd</sup> contraction stage, with  $P_0$  of (a) 100.87, (b) 10.087 and (c) 2.017.

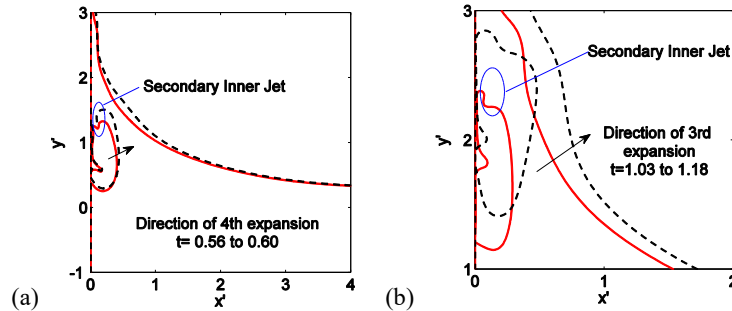


Fig. 6. Secondary inner jets in (a) 4<sup>th</sup> expansion stage with  $P_0 = 100.87$ ; (b) 3<sup>rd</sup> expansion stage with  $P_0 = 10.087$ .

#### 4 Conclusions

A multi-scale algorithm is proposed to solve the problem of wave impact on a structure using boundary element method. Dynamic details of the entrapped air cavity are captured for the case of overturning wave impact on a coastal wall. Periodic inner free jets are found to be generated on the upper cavity surface. This phenomenon is related to the negative cavity pressure at the end of its rebounding/expansion stages. The inner jets are expected to impinge the nearby surfaces, leading to the division of the cavity. This may be considered as a mechanism of the formation of rich bubbles associated with the wave impact process. More details of the techniques and results will be presented in the workshop.

#### Acknowledgement

The authors are grateful to Prof G. X. Wu from University College London for the helpful discussions on this work. We would also like to acknowledge the financial support by the National Natural Science Foundation of China (No. 51669008, 51569011, and 51709038), the support of the Fundamental Research Funds for the Central Universities (No. DUT16RC(3)113), the State Key Laboratory of Coastal and Offshore Engineering Innovation Fund for Young Scholars (No. LY17B1).

#### References

- [1] Tanizawa K, Yue DKP. Numerical computation of plunging wave impact loads on a vertical wall. Part 2. The air pocket. In: 7th Int Work on Water Waves and Floating Bodies 1992.
- [2] Zhang S, Yue DKP, Tanizawa K. Simulation of plunging wave impact on a vertical wall. *J. Fluid Mech.* 1996; 327: 221–54.
- [3] Greco M, Landrini M, Faltinsen OM. Impact flows and loads on ship-deck structures. *J Fluid Struct* 2004; 19: 251-75.
- [4] Wu GX, Sun H, He YS. Numerical simulation and experimental study of water entry of a wedge in free fall motion. *J Fluid Struct* 2004; 19: 277–89.
- [5] Mei CC. *The Applied Dynamics of Ocean Surface Waves*. Wiley-Interscience: New York; 1983.
- [6] Cooker MJ, Peregrine DH. Computations of violent motion due to waves breaking against a wall. *Proc 22nd Intl Conf Coastal Eng. Delft 1990, ASCE*; 1:164-76.
- [7] Bullock GN, Obhrai C, Peregrine DH, Bredmose H. Violent breaking wave impacts. Part 1: Results from large-scale regular wave tests on vertical and sloping walls. *Coastal Eng* 2007; 54: 602–17.